# One-Step Synthesis of Submicrometer Fibers of $MoO_3$

Greta R. Patzke,* Alexej Michailovski, Frank Krumeich, Reinhard Nesper, Jan-Dierk Grunwaldt,† and Alfons Baiker†

*Laboratory of Inorganic Chemistry, and Institute for Chemical and Bioengineering, ETH Hönggerberg, Wolfgang-Pauli-Str.10, CH-8093 Zurich, Switzerland*

*Received March 24, 2003. Revised Manuscript Received August 11, 2003*

Nanorods of $MoO_3$ are accessible in gram quantities from $MoO_3 \cdot 2H_2O$ via a flexible one-step solvothermal reaction. Several hours of treatment in water at 180 °C are sufficient to convert the starting material quantitatively into rods with diameters around 100 nm and microscale lengths. The formation of $MoO_3$ rods proceeds in both neutral ionic and acidic media within a wide parameter window encompassing reaction temperatures between 90 and 180 °C and time scales ranging from several hours to 7 d. The rod morphology can be tuned by selecting a proper additive, and the nanorods withstand heating to 400 °C. Furthermore, the reaction pathways in various solvothermal media were investigated and both intermediate molybdic acids and the bulk nanorod products were characterized by means of EXAFS spectroscopy.

## Introduction

In recent years, the "chemistry of form" has attracted considerable interest in chemistry and materials science. Not only the synthesis of inorganic materials with novel structures, but also the design of their morphology has become an important topic.[1] Pioneering work has been performed with respect to the exciting field of biomineralization,[2] and morphology control in solid state synthesis is currently explored.[3]

Principles of morphology control are pivotal for the development of a future nanotechnology.[4] During the 1990s, remarkable knowledge about the synthesis and properties of various nanomaterials and nanocomposites was achieved.[5] The fabrication of nanoscale devices requires alignment and functionalization processes, so nanoparticles with a distinct anisotropic morphology are indispensable for this purpose.[6] Nanotubes represent the most prominent examples,[7] but nanorods and nanowires have attracted considerable research interest as well.[8] They need not be stabilized by any kind of templating material and their synthesis is often surprisingly flexible and effortless.

The superconducting[9] or semiconducting[10] properties of oxidic nanorods might lead to key applications so that considerable research efforts have been undertaken to produce them in a large variety. However, there are still no general guidelines for the straightforward large-scale synthesis of oxidic nanorods with specific structures and tailor-made aspect ratios.

In this context, a novel, one-step solvothermal procedure leading to $MoO_3$ fibers has been established. Molybdenum oxides have long been known for their catalytic efficiency, e.g. in alcohol[11] and methane[12] oxidation. Manifold mechanistic studies have been conducted to facilitate the design of molybdenum oxide-based catalysts.[13] Recently, remarkable progress has been achieved concerning the preparation of low-dimensional and porous molybdenum oxide derivatives.[14] Moreover, a whole new family of molybdenum oxide-organodiamine compounds has been synthesized in the past decade.[15] Starting from structure-directing organic templates, many fascinating forms of molybdenum oxide are now available, such as molybdenum oxide fibers,[16] hollow $MoO_3$ nanospheres,[17] or mesostructured molybdenum oxide toroids.[18] Though millimeter-sized $MoO_3$ whiskers have been known for several decades,[19] their industrial preparation is still the focus of current

* Corresponding author. Tel.: +41-1-632 67 43. Fax: +41-1-632 11 49. E-mail: patzke@inorg.chem.ethz.ch.

† Institute for Chemical and Bioengineering.

(1) (a) Mann, S. *Angew. Chem., Int. Ed.* **2000**, *39*, 3392. (b) Ozin, G. A.; Yang, H.; Coombs, N. *Nature* **1997**, *386*, 692.

(2) (a) Ozin, G. A. *Acc. Chem. Res.* **1997**, *30*, 17. (b) Mann, S. *Biomineralization*; Oxford University Press: Oxford, New York, 2001.

(3) (a) Tanda, S.; Tsuneta, T.; Okajima, Y.; Inagaki, K.; Yamaya, K.; Hatakenaka, N. *Nature* **2002**, *417*, 397. (b) Patzke, G. R. *Angew. Chem., Int. Ed.* **2003**, *42*, 972.

(4) Rao, C. N. R.; Cheetham, A. K. *J. Mater. Chem.* **2001**, *11*, 2887.

(5) (a) Ajayan, P. M. *Chem. Rev.* **1999**, *99*, 1787. (b) Ajayan, P. M.; Zhou, O. Z. *Top. Appl. Phys.* **2001**, *80*, 391.

(6) Patzke, G. R.; Krumeich, F.; Nesper R. *Angew. Chem., Int. Ed.* **2002**, *41*, 2446.

(7) (a) Rao, C. N. R.; Satishkumar, B. C.; Govindaraj, A.; Nath M. *ChemPhysChem* **2001**, *2*, 79. (b) Tenne, R. *Prog. Inorg. Chem.* **2001**, *50*, 269.

(8) Pan, Z. W.; Dai, Z. R.; Wang, Z. L. *Science* **2001**, *291*, 1947.

(9) Yang, P. D.; Lieber, C. M. *Science* **1996**, *273*, 1836.

(10) (a) Duan, X.; Lieber, C. M. *Adv. Mater.* **2000**, *12*, 298. (b) Manna, L.; Scher, E. C.; Alivisatos, A. P. *J. Am. Chem. Soc.* **2000**, *122*, 12700.

(11) (a) Baiker, A.; Gasser, D. *Z. Phys. Chem.* **1986**, 149, 119. (b) Zhang, W.; Oyama, S. T. *J. Phys. Chem.* **1996**, *100*, 10759.

(12) Liu, H.-F.; Liu, R.-S.; Liew, K. Y.; Johnson, R. E.; Lunsford, J. H. *J. Am. Chem. Soc.* **1984**, *106*, 4117.

(13) (a) Baiker, A.; Dollenmeier, P.; Reller, A. *J. Catal.* **1987**, *103*, 394. (b) Ressler, J. Wienold, T.; Jentoft, R. E. *J. Catal.* **2002**, *210*, 67.

(14) (a) Oyama, S. T.; Zhang, W. *J. Am. Chem. Soc.* **1996**, *118*, 7173. (b) Guillou, N.; Férey, G.; Whittingham, M. S. *J. Mater. Chem.* **1998**, *8*, 2277.

(15) Hagrman, P. J.; Hagrman, D.; Zubieta, J. *Angew. Chem., Int. Ed.* **1999**, *38*, 2639.

(16) Niederberger, M.; Krumeich, F.; Muhr, H.-J.; Müller, M.; Nesper, R. *J. Mater. Chem.* **2001**, *11*, 1941.

(17) Liu, T.; Xie, Y.; Chu, B. *Langmuir* **2000**, *16*, 9015.

(18) Antonelli, D. M.; Trudeau, M. *Angew. Chem., Int. Ed. Engl.* **1999**, *38*, 1471.

10.1021/cm031057y CCC: $27.50 
Published on Web 02/28/2004

research activities.[20] Recently, a novel approach toward α-$MoO_3$ nanorods starting from aged ammonium heptamolybdate tetrahydrate solutions has been established.[21] In the following, a straightforward solvothermal route toward $MoO_3$ nanorods is presented that proceeds with hitherto unknown efficiency and might thus be scaled up from gram quantities to larger amounts required for technical applications:

(1) $MoO_3 \cdot 2H_2O$ is transformed quantitatively into $MoO_3$ rods within a few hours of reaction time. No side products affect the purity and uniformity of the fibrous material.

(2) The aspect ratio of the $MoO_3$ rods can be tailored easily. Certain additives exert an influence on the growth process, but mechanistic explanations have not been attained up to now.

## Experimental section

In a standard experiment, 360 mg of $MoO_3 \cdot 2H_2O$ (synthesized according to literature routes[22]), 0.4 mL glacial acetic acid, and 1.1 mL of distilled water were added to a Teflon-lined stainless steel autoclave with a capacity of 23 mL. The autoclave was then sealed, heated at 180 °C for 7 days, and subsequently cooled to room temperature. The precipitate was collected after filtration, washed with distilled water, ethanol, and ether, and dried in air. X-ray powder analysis was conducted on a STOE STADI-P2 diffractometer in transmission mode (flat sample holders, graphite-monochromated Cu Kα radiation) equipped with a position-sensitive detector (resolution ~0.01° in $2\theta$). Transmission electron microscopy (TEM) investigations were performed on a Philips CM30ST microscope operated at 300 kV ($LaB_6$ cathode). The material was deposited on a perforated carbon foil supported on a copper grid. For scanning electron microscopy (SEM), performed on a LEO 1530 (FEG) microscope with 1 kV electrons, samples were dispersed in ethanol and subsequently deposited on a silicon wafer. DTA/TG measurements were performed on a NETZSCH STA 409 C apparatus between 20 and 1200 °C with a heating rate of 10 K $min^{-1}$. Nitrogen adsorption of the molybdenum oxide fibers was measured at 77 K with an ASAP 2010 Micromeritics apparatus. Prior to the measurement, the sample was degassed at 300 °C for several hours under vacuum ($1.4 \times 10^{-3}$ Pa). The surface area was determined by the BET method. EXAFS spectra were measured in the transmission geometry at Hamburger Synchroton Labor (HASYLAB) at Deutsches Elektronensynchroton (DESY, Hamburg) at beamline ×1. Two parallel Si (311) crystals were used for monochromatization of the X-rays. By detuning the crystals to 70% of the maximum intensity, higher harmonics were effectively rejected. The EXAFS scans were recorded around the Mo K-edge between 19 600 and 21 200 eV. The raw data were energy calibrated with the help of a Mo-reference foil measured between the second and third ionization chamber, background corrected, and normalized using the WINXAS 2.1 software.[23]

## Results and Discussion

**Formation of $MoO_3$ Nanorods in Acidic Media.** In a typical procedure, $MoO_3 \cdot 2H_2O$ and diluted glacial acetic acid are subjected to 7 d of solvothermal treatment at 180 °C. The average diameter of the resulting nanorods is between 100 and 150 nm, and their length ranges from 3 $\mu$m to a maximum of 8 $\mu$m (Figure 1a). Several washing steps (water, ethanol, and acetone), followed by drying in air, afford the final product. The progress of the reaction can be monitored visually, because the yellow starting material is converted to a blue product. This indicates a slight degree of reduction in the $MoO_3$ rods which is, however, too small to be detected by standard analytical techniques.

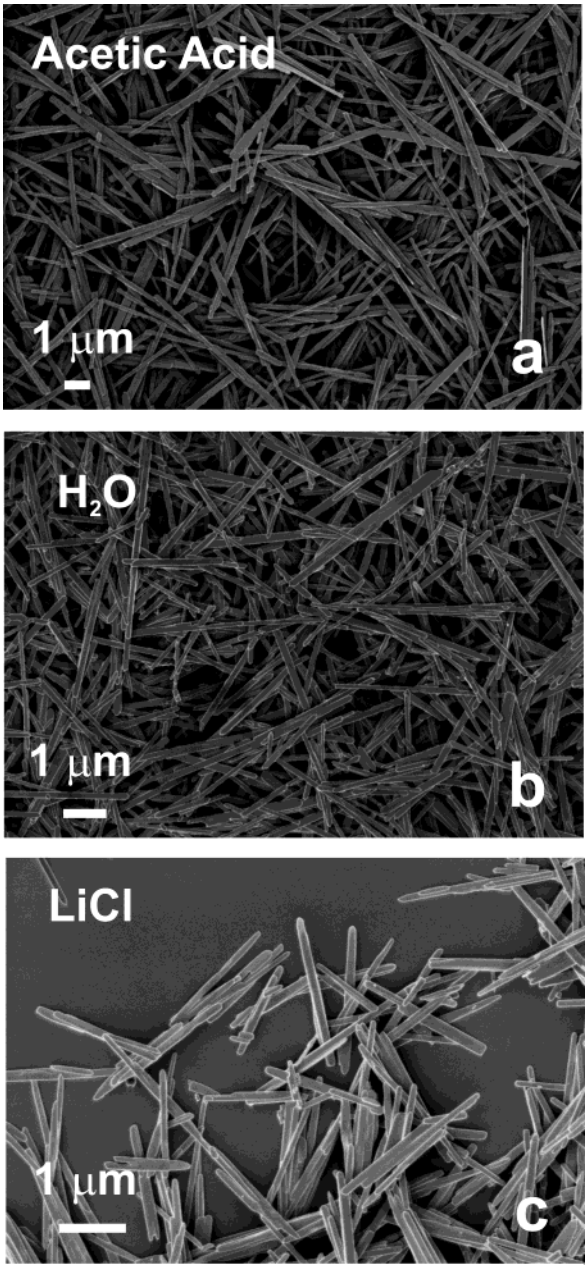


**Figure 1.** SEM images of $MoO_3$ rods grown under various conditions: (a) acidic media, (b) $H_2O$, and (c) neutral ionic media.

Subsequently, the key reaction conditions for rod formation in acidic media were explored. The presence of $MoO_3 \cdot 2H_2O$ is indispensable, because $MoO_3$ and $MoO_3 \cdot H_2O$, for example, do not afford nanorods under the above-mentioned conditions. At 180 °C, the starting material is dissolved completely, and nanorod precipitation requires at least 2 d of reaction time. The minimum reaction temperature for rod formation is 90 °C (Figure 2). Lower temperatures (80 °C) lead to dissolution of the

(19) Callahan, J. L.; Petrucci, R. H.; Brown, C. A. *Science* **1958**, *128*, 841.
(20) Li, J.; Wei, P.; Ruigang, W.; Chen, J. *Key Eng. Mater.* **2002**, *224−226*, 367.
(21) Lou, X. W.; Zeng, H. C. *Chem. Mater.* **2002**, *14*, 4781.
(22) Cruywagen, J. J.; Heyns, J. B. B. *S. Afr. J. Chem.* **1981**, *34*, 118.
(23) Ressler, T. *J. Synchr. Rad.* **1998**, *5*, 118.

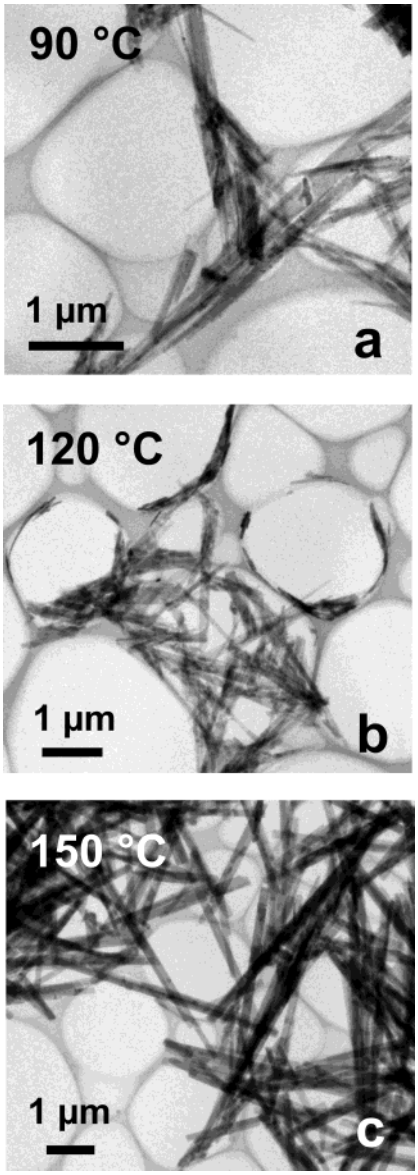


**Figure 2.** TEM images displaying the influence of the reaction temperature on the $MoO_3$ rods grown in acetic acid: (a) 90 °C, (b) 120 °C, and (c) 150 °C.

starting material without product formation. Therefore, the parameter window for nanorod formation in acetic acid is remarkably wide: the temperature can be chosen in the range between 90 and 180 °C, provided that the reaction proceeds for at least 2−3 days.

Figure 2 reveals how the reaction temperature can be used as a tuning parameter for controlling the thickness of the $MoO_3$ rods: low synthesis temperatures (90−120 °C) generate fine rods with maximum diameters of 40 nm, whereas the rods have almost reached their maximum diameter (ca. 150 nm) at 150 °C.

The effect of various acids on the rod morphology was investigated. In the first place, readily available acidic additives turned out to be most effective in terms of rod formation and morphology control. Figure 3 illustrates how the rod diameter depends on the acidic additive: weak organic acids lead to nanoscale diameters, whereas strong inorganic acids afford rods with overall microscale dimensions.

The following guideline is useful for choosing an appropriate acidic additive: the conjugated base should not inhibit $MoO_3$ precipitation by its complexation properties and it may not be incorporated into the fibers. The replacement of acetic acid by the corresponding chloroacetic acids, for example, completely inhibits rod formation. Formic acid and HBr afford rod-shaped products in a quantitative fashion, just like salicylic acid or HCl. $H_3PO_3$ and $H_3PO_4$, however, do not yield any solid products at all.

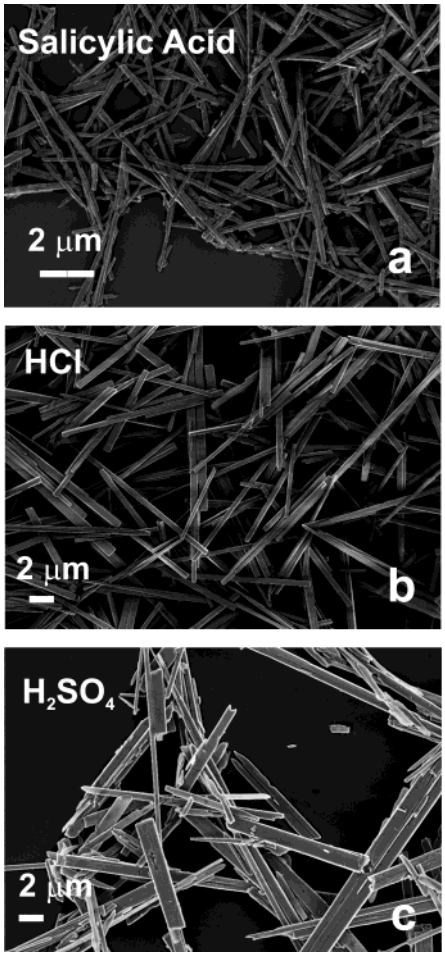


**Figure 3.** SEM images of $MoO_3$ rods with various diameters tuned by acidic additives: (a) Salicylic acid, (b) HCl, and (c) $H_2SO_4$.

In summary, the acid route to $MoO_3$ rods is a flexible and robust procedure with options for nanometer- and micrometer-scale morphology tuning together with promising features for scale-up processes.

**Formation of $MoO_3$ Nanorods in Neutral Media.** Although acidic additives are quite useful for tailoring the shape of the $MoO_3$ nanorods, their presence is not indispensable for rod formation—rods are even formed in pure water. Figure 4 reveals that a 16-h treatment of $MoO_3 \cdot 2H_2O$ in water at 180 °C results in flat rods with round ends and slightly smaller diameters (90−130 nm) than those obtained with acetic acid. Their length remains on the micron-scale and varies from 1.8 to 4 $\mu$m.

Again, the essential conditions for rod formation in water were investigated with respect to time and temperature (Figure 4). The minimum reaction temperature of 90 °C has to be maintained for 2 days of reaction time. Other than in the case of acetic acid, an intermediate can be observed at 80 °C: slightly cleaved

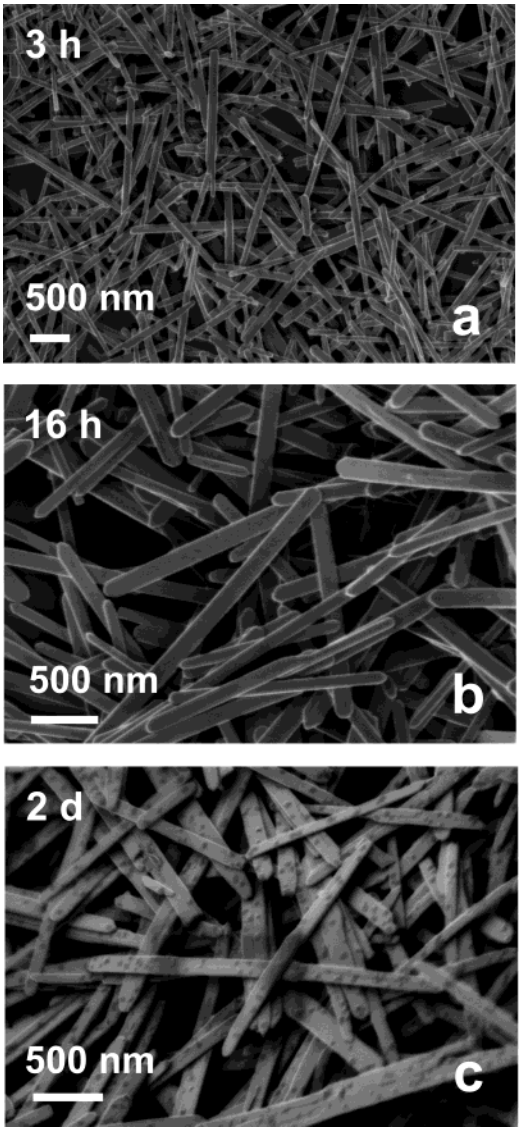


**Figure 4.** SEM images displaying the time scale of $MoO_3$ rod growth in water: (a) 3 h, (b) 16 h, and (c) 2 d.

microscale crystals of α-$MoO_3$·$H_2O$ indicate the onset of nanorod formation. The neutral and acid-based synthetic routes exhibit substantial differences concerning their time scales. Rod formation at 180 °C in water proceeds quite fast, so that a reaction time as short as 3 h is sufficient to convert the starting material quantitatively into rods. They display only a small residual degree of intergrowth (Figure 4a). Rod syntheses in water should be limited to 1 d of reaction time (Figure 4): surprisingly, after 2 days (Figure 4c)—the minimum reaction time under acidic conditions—the surfaces of the rods are covered by small holes. This suggests the onset of a dissolution process, although the XRD pattern of the rods still remains unchanged.

Following the series of the water-based experiments, the next step was to further decrease the polarity of the solvent by switching to organic media. Reactions were again performed under standard conditions (2 d, 180 °C) employing toluene, hexane, mesitylene, cyclohexane, naphthalene, and $CHCl_3$. The overall trend is clear: rather nonpolar organic solvents initiate the formation of $MoO_3$ rods, but the reaction does not proceed completely. With all the organic solvents investigated, rod

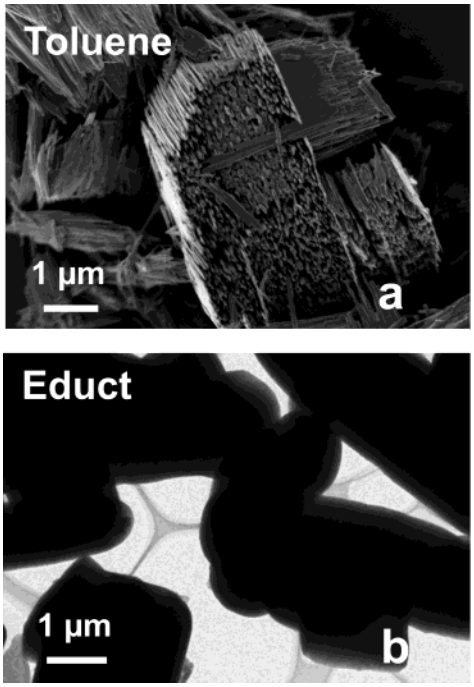


**Figure 5.** (a) SEM image of $MoO_3$ rod bundles formed in the presence of toluene as a nonpolar medium, and (b) TEM image of the starting material as a reference.

formation is stopped before the separation step so that bundles of aggregated rods are generated. In the case of toluene, a remarkable degree of alignment is obtained in bundles consisting of nanorods with an average diameter around 50 nm. There is no evidence, however, of any prestructuring in the starting material (Figure 5).

Finally, $MoO_3$·$2H_2O$ was reacted for 2 d at 180 °C under autogenous pressure in the absence of a solvent. Again, bundle-like structures made up of rods with diameters between 50 and 100 nm were formed. Similar to the reaction in water, the formation of $MoO_3$·$0.33H_2O$ as an intermediate could be monitored at 90 °C. The microcrystals already exhibit a certain degree of cleavage, indicating the formation of nanoscale rods. Thus, the common onset temperature for nanorod formation appears to be around 80−90 °C for acetic acid, water, and unpolar solvents and for the bulk solid form.

In summary, to generate highly anisotropic $MoO_3$ particles in a quantitative fashion, a protic or polar solvent has to be employed at reaction temperatures above 100 °C. Nonpolar solvents favor the association of rods into bundles (Figure 5a).

**Formation of $MoO_3$ Rods in the Presence of IonicMedia.** It is well-known that soluble additives can be employed for systematic morphology control in crystal growth processes. The change of the rhombohedral habit of calcite ($CaCO_3$) crystals to a platelet form in the presence of $Li^+$ ions is an instructive example: the ion additive adsorbs specifically on the {001} planes, inhibiting the growth of these faces.[1] The solvothermal interaction of $MoO_3$·$2H_2O$ with alkali/alkaline earth halides has been explored in the course of a systematic study, and the main results concerning the additive-controlled synthesis of $MoO_3$ nanorods are summed up in the following.[24]

Two categories of additives could be differentiated: the first group includes those additives that exert

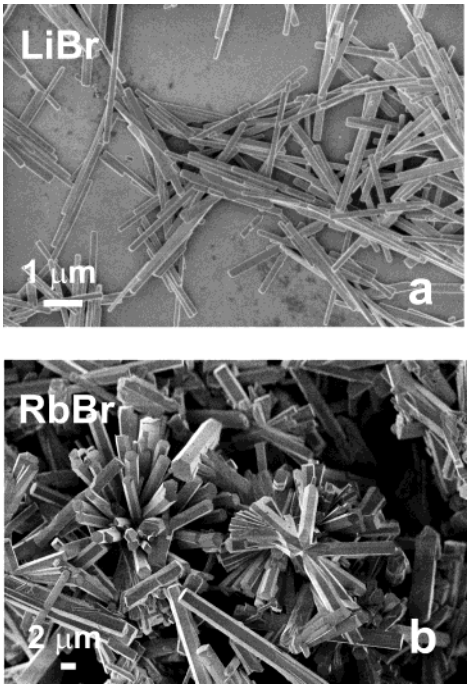


**Figure 6.** SEM images: LiBr and RbBr represent two classes of additives leading to either $MoO_3$ rod formation (a) or a hexagonal molybdate phase (b).

morphology control by adsorption processes during crystal growth or that act via affecting the ionic strength of the medium. Additives belonging to the second category participate in a chemical reaction with the starting material and thus lead to the formation of alkali molybdates with a well-developed morphology on the micron-scale.

Among the alkali chlorides and bromides, for example, LiCl or LiBr unambiguously represent the first additive category and favor the formation of $MoO_3$ rods with shapes different from the standard, additive-free procedures (Figures 1c and 6a). LiCl induces a decrease in aspect ratio compared to the standard acetic acid routine (Figure 1c), together with a slightly shortened average diameter (around 90 nm). LiBr exerts a similar influence on the aspect ratio (Figure 6a). Among the chloride-based ionic additives, the opportunity of morphology control is even more evident. The use of $MgCl_2$ and $CaCl_2$ instead of LiCl leads to a considerable decrease in aspect ratio of the emerging rod-shaped $MoO_3$ particles (Figure 7). The average diameter around 100 nm increases by a factor of about 3 to 340 nm when $CaCl_2$ is employed as an additive.

Additives belonging to the remaining MX series (M = Na−Cs, X = Cl, Br), however, participate actively in the reaction with $MoO_3 \cdot 2H_2O$ and lead to the formation of hexagonal molybdates that are structurally closely related to the $AH_{6x-1}Mo_{6-x}O_{18}$ (A = Na, K, $NH_4$) series.[25] They adopt a rod-shaped hexagonal crystal habit and exhibit a tendency toward bundle-like ordered arrangements. The flower-like hexagonal molybdate crystals grown in the presence of RbBr might serve as an example (Figure 6b). Such metastable hexagonal molybdates with a tunnel-like open framework, including mobile alkali cations, have attracted considerable interest as precursors for the long-sought-after hexagonal form of $MoO_3$.[26]

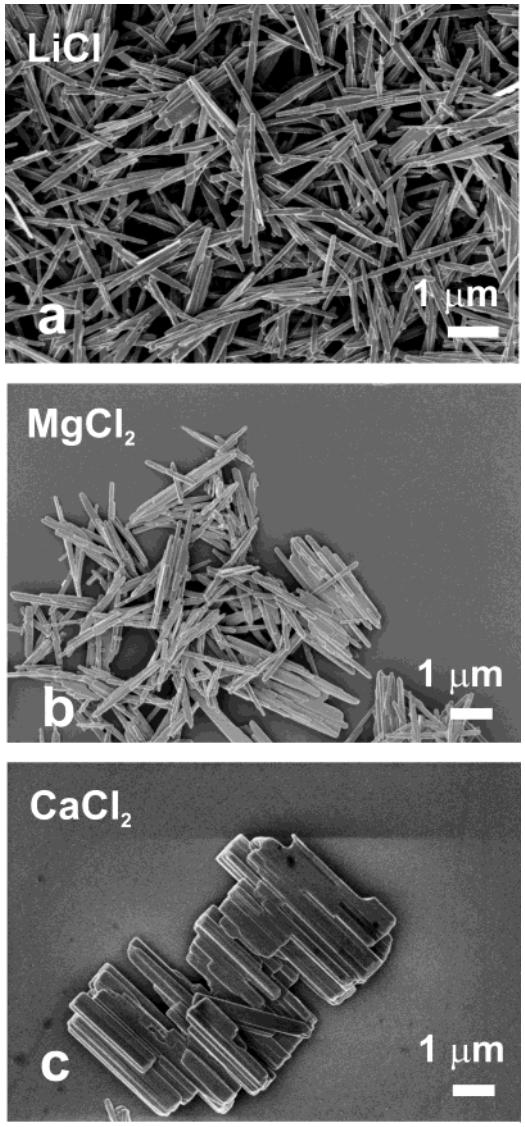


**Figure 7.** Both alkali and earth-alkali chlorides are suitable additives for morphology control of $MoO_3$ (SEM images): (a) LiCl, (b) $MgCl_2$, and (c) $CaCl_2$.

**Thermal Behavior of $MoO_3$ Rods.** To investigate the thermal stability of the rod-shaped material, a sample of $MoO_3$ rods synthesized in the presence of LiBr was heated in air for 8 h at 400 °C. Figure 8 clearly reveals that the morphology remains entirely unaltered so that the material might be suitable for applications at elevated temperatures. Moreover, the crystallinity of the rods is improved, because the peak width in the XRD pattern of the thermally treated material is reduced considerably.

The $N_2$ Brunauer−Emmett−Teller (BET) surface area of a $MoO_3$ rod sample fabricated by the standard acetic acid routine was found to be 13.4 $m^2\ g^{-1}$, confirming the absence of a porous structure, which would

(24) Michailovski, A.; Krumeich, F.; Patzke, G. R. Submitted to *Helv. Chim. Acta*.

(25) McCarron, E. M., III; Thomas, D. M.; Calabrese, J. C. *Inorg. Chem.* **1987**, *26*, 370.

(26) (a) Guo, J.; Zavalij, P.; Whittingham, M. S. *J. Solid State Chem.* **1995**, *117*, 323. (b) Guo, J.; Zavalij, P.; Whittingham, M. S. *Eur. J. Solid State Inorg. Chem.* **1994**, *31*, 833.

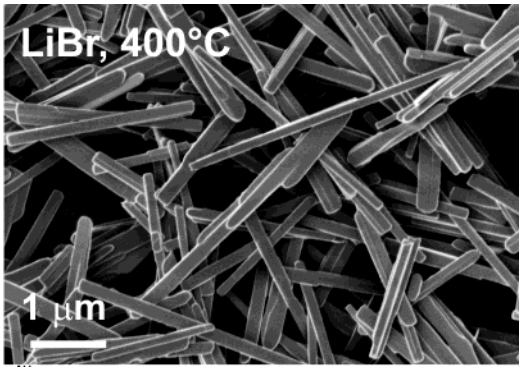


**Figure 8.** SEM images of $MoO_3$ rods (cf. Figure 6 a) after treatment at 400 °C (8 h, air).

result in much higher BET surfaces (up to ca. 100 $m^2 g^{-1}$).[27]

**X-ray Absorption Spectroscopy of $MoO_3$ Nanorods and of the Corresponding Intermediate Molybdic Acids.** Selected $MoO_3$ rods with diameters covering the micro- and the nanoscale (Figure 9, Table 1) as well as the two molybdic acids α-$MoO_3 \cdot H_2O$ and $MoO_3 \cdot 0.33H_2O$ occurring as intermediates on their way to rod-shaped products (Figure 13) were investigated by extended X-ray absorption spectroscopy at the Mo K-edge, which has proven useful in previous studies.[28] Both α-$MoO_3$ and most of the molybdic acids known so far exhibit $MoO_6$ octahedra as the characteristic local structural feature, which are arranged in layers (cf. Figure 12). Therefore, the Mo−O bond distances observed for this class of compounds can be grouped into three subsets: the terminally bound oxygen is positioned perpendicular to the direction of the planes and exhibits a rather short Mo−O bond distance around ∼1.69 Å. The bridging Mo−O bonds of the octahedral units involve four oxygen atoms leading to intermediate Mo−O distances ranging from 1.73 to 2.25 Å. Finally, the remaining sixth oxygen atom (Mo−O distances 2.29−2.34 Å) is located opposite to the terminally bound oxygen atom and belongs either to a weakly bound water molecule or it represents another bridging atom. Note that the local structure around the central molybdenum atom is quite similar for the series $MoO_3 \cdot 2H_2O \rightarrow$ α-$MoO_3 \cdot H_2O \rightarrow MoO_3 \cdot 0.33H_2O \rightarrow MoO_3$, and at first glance, similar EXAFS/Fourier transformed EXAFS spectra should be expected. Multiple scattering (MS) paths, however, play an important role. Such multiple scattering effects[29] have been studied for samples such as $ReO_3$,[30,31] $WO_{3-x}$,[31] $FeF_3$,[31,32] and $MoO_3$.[33] The scattering amplitude and the phase shift change with the bond angle in the Mo−O−Mo chains. In perovskites and $MoO_3$, the MS paths are strong in intensity if the chain is linear, and thus, important information on the structure can be obtained. This phenomenon in a linear or near-linear geometry has been described as the "focusing effect".[31, 32, 34]

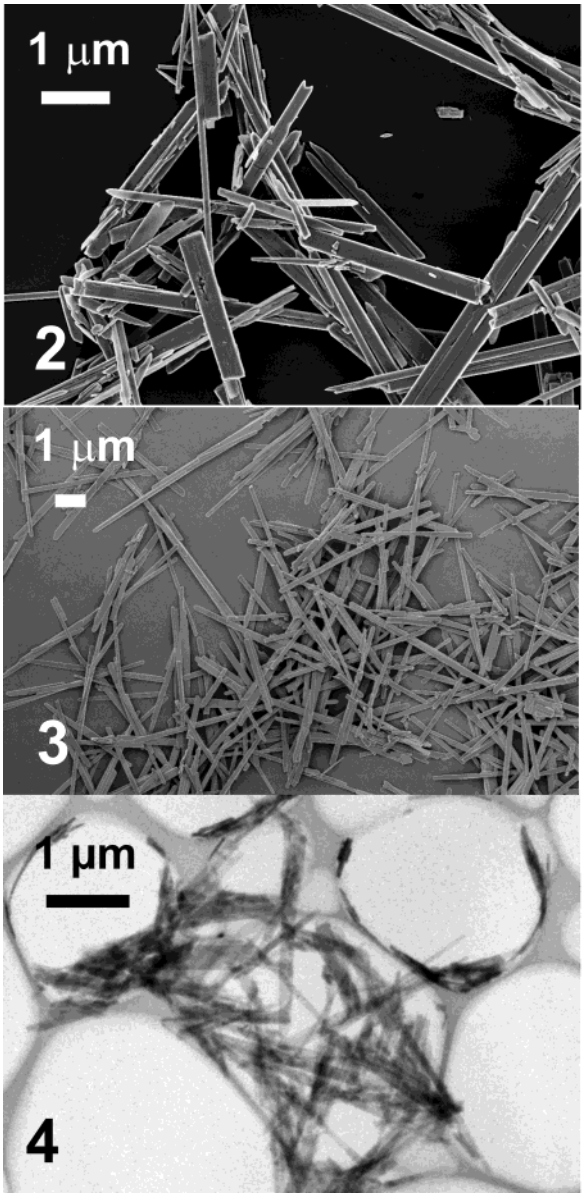


**Figure 9.** $MoO_3$ rods with various diameters and aspect ratios employed in EXAFS investigations (cf. Figures 10 and 11).

**Table 1. Size Distributions of the $MoO_3$ Rod Particles (cf. SEM and TEM images in Figure 9) Subjected to EXAFS Investigations**

| sample | average length/μm | average diameter/nm |
|---|---|---|
| 2 | 8−10 | 700 |
| 3 | 4−5 | 140 |
| 4 | 1−2.5 | 40 |

In Figure 10 the normalized X-ray absorption near-edge structures (XANES) are shown for $MoO_3$ rods of several sizes together with commercial, polycrystalline

(27) Nazar, L. F.; Liblong, S. W.; Yin, X. T. *J. Am. Chem. Soc.* **1991**, *113*, 5889.
(28) (a) Ressler, T.; Timpe, O.; Neisius, T.; Find, J.; Mestl, G.; Dieterle, M.; Schlögl, R. *J. Catal.* **2000**, *191*, 75. (b) Ressler, T.; Wienold, J.; Jentoft, R. E.; Neisius, T. *J. Catal.* **2002**, *210*, 67.
(29) Sahiner, A.; Crozier, E. D.; Jiang, D. T.; Ingalls, R. *Phys. Rev. B* **1999**, *59*, 3902. (b) Della Longa, S.; Arcovito, A.; Girasole, M.; Hazemann, J. L.; Benfatto, M. *Phys. Rev. Lett.* **2001**, *87*, 155501−1.
(30) Houser, B.; Ingalls, R. *Phys. Rev. B* **2000**, *61*, 6515.
(31) (a) Kuzmin, A.; Purans, J.; Parent, Ph. *Physica B* **1995**, *208−9*, 45. (b) Kuzmin, A.; Purans, J. *J. Phys.: Condens. Matter* **1993**, *5*, 9423.
(32) Kuzmin, A.; Parent, Ph. *J. Phys.: Condens. Matter* **1994**, *6*, 4395.
(33) Kuzmin, A.; Purans, J. *J. Phys.: Condens. Matter* **2000**, *12*, 1959.
(34) (a) Sperandini, F.; Di Cicco, A.; Gazda, M. *Phys. Rev. B* **1998**, *57*, 6067. (b) Díaz-Moreno, S.; Muñoz-Páez, A.; Sánchez Marcos, E. *J. Phys. Chem. B* **2000**, *104*, 11794.

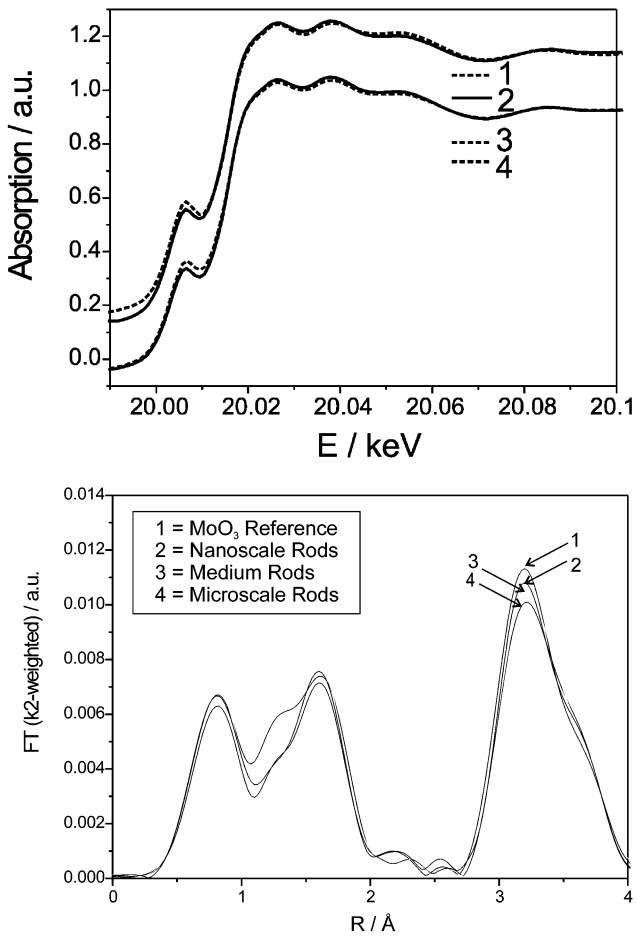


**Figure 10.** XANES spectra of $MoO_3$ nanorods (above) and Fourier transforms of the $MoO_3$ rod XANES spectra (below).

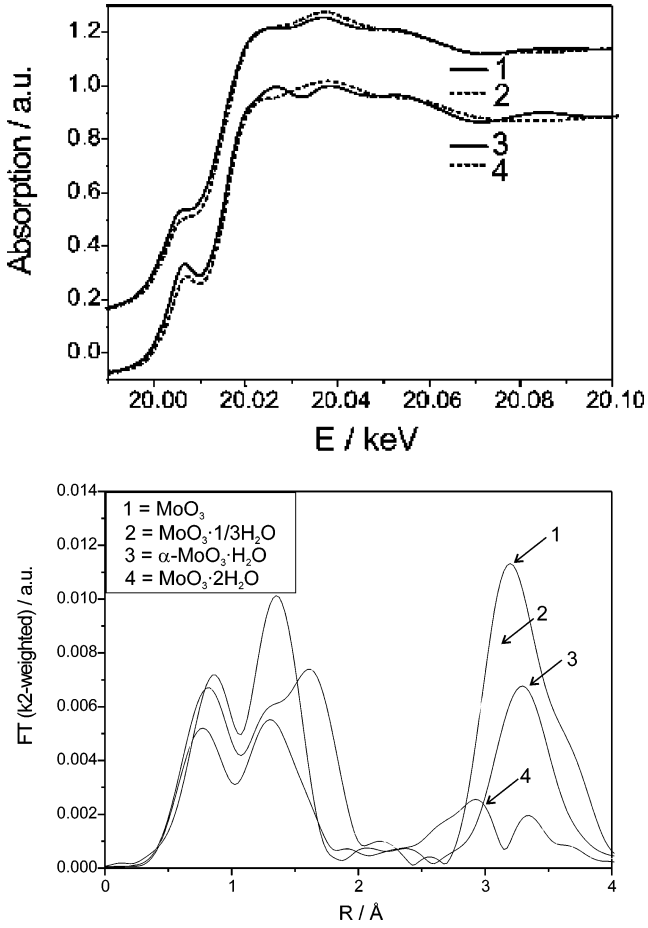


**Figure 11.** XANES spectra of molybdenum oxide hydrates (above) and Fourier transforms of the XANES spectra (below).

$\alpha$-$MoO_3$ powder as a reference, and their Fourier transforms (FTs) are compared. First, it is evident from the spectra that the $MoO_3$ rods of all sizes unambiguously adopt the structure of $\alpha$-$MoO_3$. Moreover, the first shell exhibits several species (peaks below 2 Å in the Fourier transformed spectra). They reflect the above-mentioned presence of different types of molybdenum−oxygen bonding with the characteristic variation of Mo−O bond lengths and thus agree well with literature data.[28,33] Furthermore, different amplitudes of the outer shell peaks (indicated by arrows in Figure 10) are observed that point to differences in crystallite size. Indeed, the amplitude increases with the particle size of the $MoO_3$ rods (Figure 9), thereby confirming the trends described in former studies on the subject,[33] together with a successful size tuning of the rods throughout the complete bulk material.

Figure 11 displays the XANES spectra of $\alpha$-$MoO_3 \cdot H_2O$ and $MoO_3 \cdot 0.33H_2O$ together with commercial $MoO_3$ and the starting material $MoO_3 \cdot 2H_2O$ as references. The pre-edge shoulder of all compounds indicates some structural differences, because it is known to depend on the symmetry and thus reflects the degree of distortion in the $MoO_6$ octahedra. For a perfect octahedron, such a transition is forbidden in the dipole approximation.[33] The changes of the Mo−$O_I$, Mo−$O_{II}$, and Mo−$O_{III}$ distances can also be observed in the $k^2$-weighted Fourier transformed spectra in Figure 11 (below). Most noticeable, however, is the increasing amplitude of the second shell (indicated with 1−4 in Figure 11) derived from the Fourier transformation of the corresponding XAFS signals. In a former XAFS study on the $MoO_3 \cdot 2H_2O \rightarrow \beta$-$MoO_3 \cdot H_2O \rightarrow MoO_3$ series, an analogous effect was reported.[33] $\beta$-$MoO_3 \cdot H_2O$ represents another form of molybdenum oxide monohydrate arising from a topotactic dehydration of $MoO_3 \cdot 2H_2O$.[35] Its exact crystal structure has not been determined up to now. EXAFS gives, however, due to the variation of second shell amplitudes, a direct indication of the presence of near-linear Mo−O−Mo chains. Only these give rise to strong multiple-scattering (MS) signals contributing to FTs beyond the first shell. The increase in second shell intensity in the $MoO_3 \cdot 2H_2O \rightarrow \beta$-$MoO_3 \cdot H_2O \rightarrow MoO_3$ series thus reveals that the Mo−O−Mo angle along one of the crystallographic axes increases in this series.

The apparent trend in second-shell amplitudes in the present investigation can thus be explained in terms of the increasing tendency of the molybdic acids toward formation of the above-mentioned near-linear Mo−O−Mo chains with decreasing water content (cf. Figure 12).

While the crystal structure of $MoO_3 \cdot 2H_2O$[36] does not display any such chains, $\alpha$-$MoO_3 \cdot H_2O$ exhibits Mo−O−Mo chains running along the *c* axis with a value of 143° for the Mo−O−Mo angle,[37] leading to an increase in amplitude compared to $MoO_3 \cdot 2H_2O$.

A further increase in intensity observed in $MoO_3 \cdot 0.33H_2O$ can be attributed to a widening of the Mo−

(35) Günter, J. R. *J. Solid State Chem.* **1972**, *5*, 354.
(36) Krebs, B. *Acta Crystallogr.* **1972**, *B28*, 2222.
(37) Böschen, I.; Krebs, B. *Acta Crystallogr.* **1974**, *B30*, 1795.

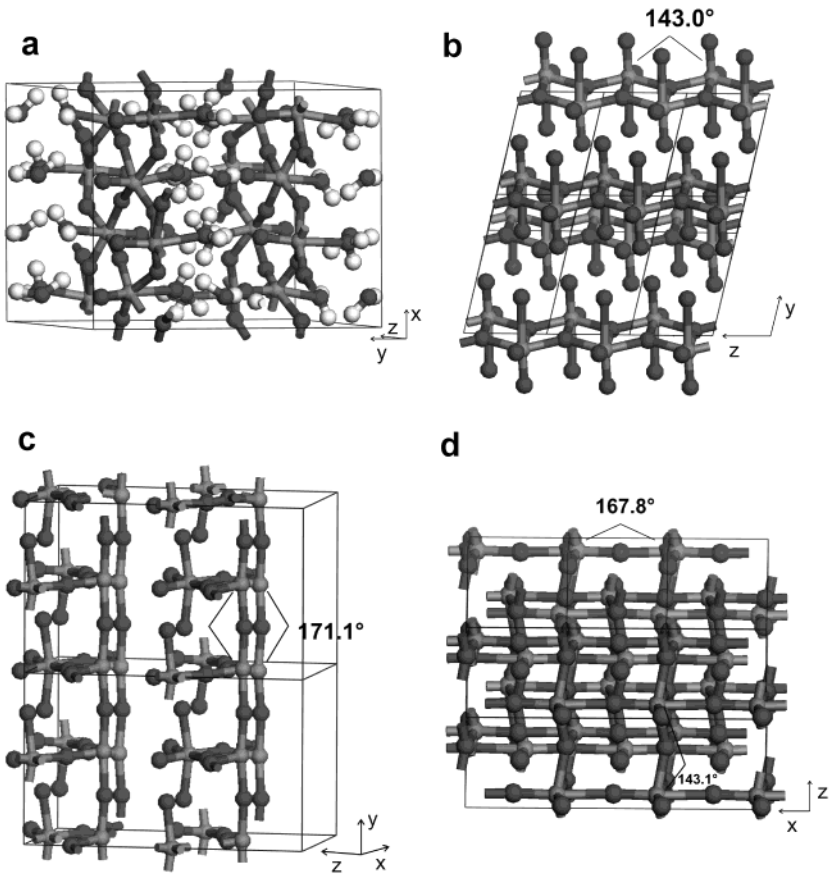


**Figure 12.** Crystal structures of (a) $MoO_3 \cdot 2H_2O$, (b) $\alpha$-$MoO_3 \cdot H_2O$, and (c) $MoO_3 \cdot 0.33H_2O$ compared to molybdenum oxide (d) displaying the increasing tendency toward the formation of linear Mo−O−Mo chains.

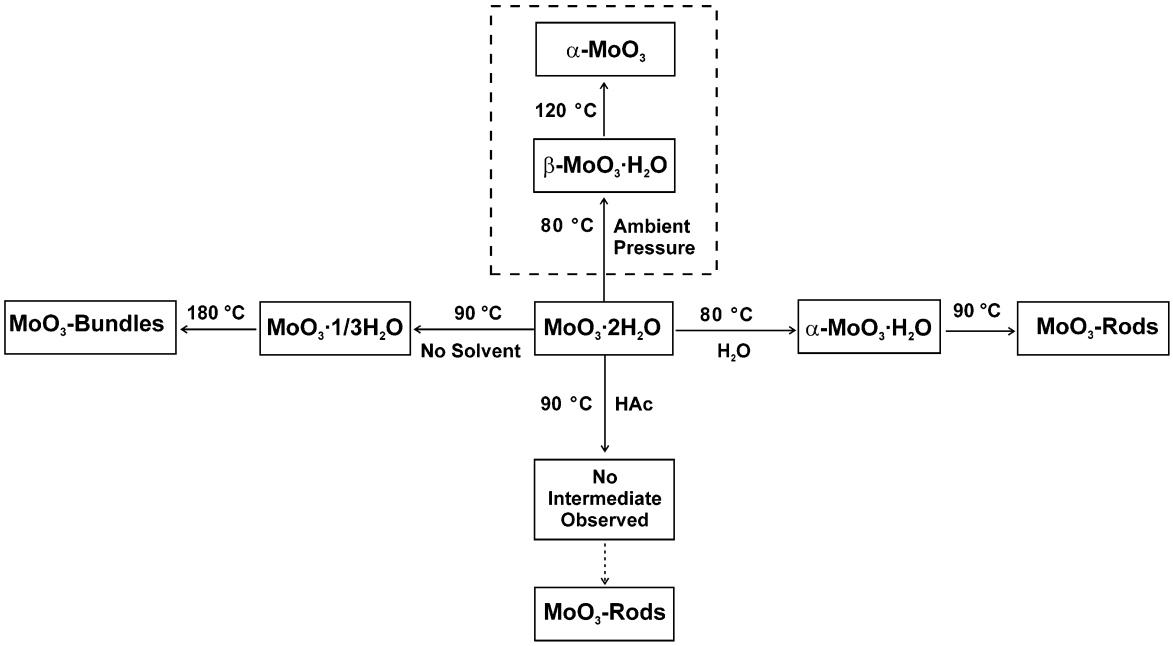


**Figure 13.** Pathways of rod formation in different reaction media.

O−Mo angle (171° in chains following the *b* direction).[38] Finally, $MoO_3$ yields maximum intensity due to the presence of two different sorts of chains along the *a* and *c* axis with Mo−O−Mo angles of 143° and 168°, respectively.[39]

In summary, XAFS studies have been proven to be a valuable tool for the elucidation of structural details in

(38) Seguin, L.; Gérand, B.; Chevrier, G.; Touboul, M. *Mater. Sci. Forum* **1996**, *228−231*, 695.

(39) Kihlborg, L. *Ark. Kemi* **1963**, *21*, 357.

molybdic acids as intermediates formed on the way toward nanorods. Moreover, the size-tuning of $MoO_3$ rods can be confirmed for the entire bulk material.

## Discussion

Figure 13 outlines the various reaction pathways leading to the formation of nanostructured material from $MoO_3 \cdot 2H_2O$. The starting material exhibits a layered structure made up of $[MoO_5(H_2O)]$ octahedra connected to infinite layers that are separated by intercalated and differently bound water molecules.[36] Their subsequent removal in two steps occurs topotactically when $MoO_3 \cdot 2H_2O$ is slowly heated to 125 °C in air.[35]

Concerning the various solvothermal pathways leading to $MoO_3$ rods, it would be reasonable to assume that at least one of them corresponds to the above-mentioned formation of $MoO_3$ from $MoO_3 \cdot 2H_2O$ proceeding via $\beta$-$MoO_3 \cdot H_2O$ as an intermediate.[40] The latter, however, is involved in none of the mechanisms investigated here. Instead, $\alpha$-$MoO_3 \cdot H_2O$ and $MoO_3 \cdot 0.33H_2O$ occur as intermediates in water and in the bulk solid reaction, respectively. Thus, the conventional topotactic dehydration scheme is altered considerably in neutral solvothermal media. Especially $MoO_3 \cdot 0.33H_2O$ is more likely to generate $MoO_3$ in the $\beta$-form first, but the $\alpha$-form present in the rods is the immediate dehydration product.[40]

The most striking feature of the reaction pathway in water is the highly spontaneous character of the dehydration reaction of $MoO_3 \cdot 2H_2O$, which affords $MoO_3$ rods within less than 3 h (Figure 4). According to thermodynamic considerations, water loss should be less favorable in aqueous media, and therefore, it cannot represent the driving force of the reaction in the first place.

Finally, no intermediate at all could hitherto be isolated during rod formation in acidic media. This points to a dissolution−precipitation sequence, which does not include any topotactic steps. Certainly, this hypothesis has to be confirmed, and appropriate in situ EXAFS investigations are under way. There is apparently no direct topochemical link between the layered structure of the starting material and the anisotropic morphology of the product in acidic media. Consequently, a considerably widened spectrum of potential educts with a nonlayered structure might give access to a multitude of anisotropic materials via related solvothermal routes.

The morphology tuning options of this nanorod synthesis could clearly be confirmed for the bulk material by means of EXAFS spectroscopy. EXAFS also turned out to be a useful tool for a more detailed structural characterization of the intermediate molybdic acids on their way to $MoO_3$ nanorods. Their tendency toward formation of linear Mo−O−Mo chains increases with decreasing water content, so dehydration products with an anisotropic morphology are favored.

Concerning neutral ionic media, the careful selection of ionic additives permits one either to design the resulting rod shape or to change the course of the reaction completely to produce various molybdates with novel modifications among them.[24]

## Conclusion

A one-step synthetic routine leading to fibrous $MoO_3$ has been established that can be adjusted by the choice of readily accessible acidic or ionic additives to generate rod-shaped particles displaying a wide range of shapes and aspect ratios. Moreover, these reactions proceed almost quantitatively under rather mild solvothermal conditions starting from yellow molybdic acid as a readily available and stable precursor material. Due to the ease of preparation and the thermal stability of the $MoO_3$ rods that are now available at least in gram quantities, this newly established synthetic method could become a valuable starting point for generating materials for practical applications, such as in sensor technology or catalysis. For catalytic applications, a high surface area is required and an extension to mixed oxides would be favorable.

**Acknowledgment.** Our research was supported by the ETH Zurich, by the Swiss National Science Foundation (MaNEP-Materials with Novel Electronic Properties), and by the National Research Program "Supramolecular Functional Materials". The authors thank Dr. Christoph Stinner for the BET measurements. We also thank the Hamburger Synchroton Labor (HASYLAB) at Deutsches Elektronensynchroton (DESY) for beamtime and support.

CM031057Y

(40) Figlarz, M. *Prog. Solid State Chem*. **1989**, *19*, 1.